Journal of Materials Chemistry A

Accepted Manuscript

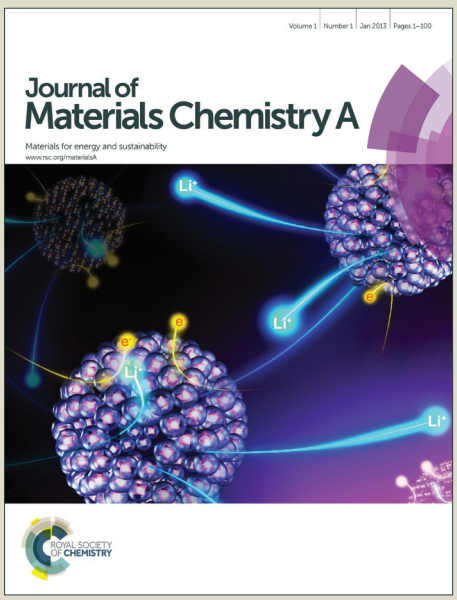

This is an *Accepted Manuscript*, which has been through the Royal Society of Chemistry peer review process and has been accepted for publication.

Accepted Manuscripts are published online shortly after acceptance, before technical editing, formatting and proof reading. Using this free service, authors can make their results available to the community, in citable form, before we publish the edited article. We will replace this *Accepted Manuscript* with the edited and formatted *Advance Article* as soon as it is available.

You can find more information about *Accepted Manuscripts* in the Information for Authors.

Please note that technical editing may introduce minor changes to the text and/or graphics, which may alter content. The journal's standard Terms & Conditions and the Ethical guidelines still apply. In no event shall the Royal Society of Chemistry be held responsible for any errors or omissions in this *Accepted Manuscript* or any consequences arising from the use of any information it contains.

ROYAL SOCIETY OF CHEMISTRY

www.rsc.org/materialsA

Draining the Photoinduced Electrons Away from anode: the Preparation of Ag/Ag_3PO_4 Composite Nanoplate Photoanode for Highly Efficient Water Splitting

Qingyong Wu[a], Peng Diao[a,*], Jie Sun[a], Di Xu[a], Tao Jin[a,b], Min Xiang[a]

[a]*Key Laboratory of Aerospace Materials and Performance (Ministry of Education), School of Materials Science and Engineering, Beihang University, Beijing 100191, P.R.China*

[b]*China Special Vehicle Research Institute, Aviation Key Laboratory of Science and Technology on Structural Corrosion Prevention and Control, Jingmen 448035, Hubei, P.R.China*

*Corresponding author. Tel +86-10-8233 9562. E-mail address : pdiao@buaa.edu.cn

Abstract

The Ag/Ag_3PO_4 composite nanoplate photoanodes were fabricated by electrogeneration of Ag_3PO_4 on the surface of the vertically aligned Ag nanoplates (NPs) in phosphate solution. The outside Ag_3PO_4 layer acted as light-absorbing material to generate the electron-hole pairs, while the inside Ag NPs acted as both the framework and the electrical connector between Ag_3PO_4 and the conducting substrate. The obtained composite photoanodes showed a high catalytic activity toward photoelectrochemical (PEC) oxygen evolution reaction (OER). The photoinduced holes reacted with water to generate oxygen on Ag_3PO_4 surface, while the photoinduced electrons were efficiently transported to the counter electrode by the highly conductive Ag NPs. The Ag/Ag_3PO_4 composite photoanode exhibited a photocurrent density of 0.25 $mA \cdot cm^{-2}$ at 0.500 V *vs.* SCE, which is the highest in reported values obtained under

Journal of Materials Chemistry A Accepted Manuscript

conditions similar to this work. The amount of evolved oxygen was monitored to evaluate the percentage of the photocurrent involved in PEC OER, and the Faraday efficiency for PEC OER was obtained to be *ca.* 95.6%, indicating most of the photoinduced holes were engaged in OER. The *in situ* PEC oxidation of Ag to Ag_3PO_4, which compensated the loss of Ag_3PO_4 during PEC OER, makes the Ag/Ag_3PO_4 composite a self-healing system for OER in phosphate solution.

KEYWORDS: vertically aligned silver nanoplate, silver orthophosphate, composite photoanode, photoelectrochemical water splitting, oxygen evolution reaction

1. Introduction

Solar-powered water splitting has attracted great attention for decades because it converts solar energy into chemical energy without producing any pollution and wastes [1-4]. Great efforts have been made to develop highly efficient water-splitting catalyst since Honda and Fujishima first demonstrated that titanium dioxide could be employed as a catalyst to split water into H_2 and O_2 under UV irradiation [5]. Solar-powered water-splitting involves two half-cell reactions, the hydrogen evolution reaction (HER) and the oxygen evolution reaction (OER). The latter is more complex and sluggish because it involves the removal of four electrons and two protons from two H_2O molecules [6]. In principal, semiconductors with valence band edge more positive than the potential of the O_2/H_2O redox couple (1.23 V *vs.* NHE) can be used as photocatalysts to generate oxygen from water [7].

Journal of Materials Chemistry A Accepted Manuscript

Silver orthophosphate (Ag_3PO_4) is a n-type semiconductor [8] with a direct bandgap of 2.43 eV as well as an indirect transition of 2.36 eV, which ensures that Ag_3PO_4 absorbs solar energy with a wavelength shorter than ca. 530 nm. The valence band edge of Ag_3PO_4 is located at ca. 2.85 V *vs.* NHE [8, 9], which is much higher than the potential of the O_2/H_2O redox couple (1.23 V *vs.* NHE), ensuring that the photogenerated holes in the valence band of Ag_3PO_4 have enough energy to oxidize water. In principle, Ag_3PO_4 can be used as photoanode material to catalyze many oxidation reactions, such as OER and oxidation of organic pollutants. It has been reported that Ag_3PO_4 can be used as a catalyst for oxidative photodegradation of organic dyes [10-14]. Recently, Ye's group demonstrated that Ag_3PO_4 also acted as a promising photocatalyst for OER [8]. They showed that, with $AgNO_3$ as the sacrificial reagent for photogenerated electrons, Ag_3PO_4 exhibited even much higher photoactivity toward OER than WO_3 and $BiVO_4$, and the latter two have been well-recognized as two efficient OER photocatalysts [15-20]. However, not much work has been reported on using Ag_3PO_4 as a catalyst for photoelectrochemical (PEC) water splitting [8, 9], and there is room for further improving its photo-to-oxygen conversion efficiency.

The high electron-hole recombination rate, the instability, and the slight solubility of Ag_3PO_4 are three factors that impede the improvement of the photo-to-oxygen conversion efficiency and the long-term stability. Firstly, the low electron conductivity of Ag_3PO_4 makes it difficult for the photoinduced electrons to be efficiently drained away from Ag_3PO_4 to the cathode. As a result, electrons will accumulate in the conduction band of Ag_3PO_4 when the photoinduced holes oxidize water at Ag_3PO_4/solution interface [21]. Just like in many other n-type photoanode materials [22-24], accumulation of electrons negatively shifts the

Journal of Materials Chemistry A Accepted Manuscript

conduction band potential and then decreases the potential across the space charge region, which is the driving force for electron-hole separation. Moreover, electron accumulation greatly increases the electron-hole recombination rate, and then decreases the photo-to-oxygen conversion efficiency. Secondly, Ag_3PO_4 is not quite stable especially when the electrons accumulate in the conduction band of Ag_3PO_4 because Ag_3PO_4 can be reductively decomposed by photoinduced electrons [14, 25-27]. Therefore, fast extraction of electrons from Ag_3PO_4 is of great significance to improve both the activity and the stability of Ag_3PO_4. However, in most cases, highly active Ag_3PO_4 nanoparticles were synthesised in homogeneous solution [21, 28, 29], the deposition approach used to deposit Ag_3PO_4 onto the electrode usually did not guarantee a good electron conductivity between Ag_3PO_4 and the conductive substrates. Finally, Ag_3PO_4 is slightly soluble in water (K_{sp} = 8.89×10^{-17}) [30], which means that part of Ag_3PO_4 will slowly dissolve into the electrolyte during the long-term PEC reaction [9, 29, 31, 32]. This undermines the long-term PEC activity and stability of Ag_3PO_4 as a photoanode material. According to the above discussion, it is highly desirable both to grow Ag_3PO_4 directly on the surface of a conductive network, which allows fast extraction of photoinduced electrons from Ag_3PO_4 to the cathode, and to create a self-healing Ag_3PO_4 system [8], which improves the long-term stability and inhibits the dissolution of Ag_3PO_4.

Many studies focused on the morphology-controlled synthesis of Ag nanostructures on conducting substrates.[33-35] Inspired by these works, we came up with the idea to first fabricate a high-specific-area Ag nanostructure network and then transform the surface Ag to Ag_3PO_4 to obtain Ag/Ag_3PO_4 composite. On the basis of this idea, we developed an

Journal of Materials Chemistry A Accepted Manuscript

electrodeposition method to prepare vertically aligned Ag nanoplate (NP) arrays on indium tin oxide (ITO) substrate. Then, the ITO-supported Ag NPs were electrochemically oxidized in phosphate solution to generate an Ag_3PO_4 layer on the surface of Ag NPs. The resulting Ag/Ag_3PO_4 composite have two inherent advantages for PEC OER: (1) The aligned NP structure provides a large specific area that benefits not only the light absorption but also the charge transfer reaction at Ag_3PO_4/solution interfaces. (2) The inner Ag NPs act as efficient connectors between Ag_3PO_4 and the ITO substrate, which facilitates electron-hole separation by fast extraction of photoinduced electrons from Ag_3PO_4. (3) The Ag/Ag_3PO_4 composite is a self-healing catalyst for PEC OER in phosphate solution due to the *in situ* supply of Ag_3PO_4 by oxidation of surface Ag. In fact, the composite photoanode exhibited high activity and good stability, showing a photocurrent density of 0.25 $mA \cdot cm^{-2}$ at a bias of 0.500 V *vs*. SCE. The Faraday efficiency for OER at the composite photoanode was as high as 95.6%, indicating that most of the photocurrent was involved in PEC OER.

2. Experimental section

2.1 Fabrication of Ag nanoplate (NP) arrays

As illustrated schematically in Fig. 1, the vertically aligned Ag NP arrays were prepared by a double-potential-step electrodeposition on a CHI 660D electrochemical workstation. The electrodeposition was carried out in a three-electrode cell with a Pt foil and a saturated calomel electrode (SCE) as the counter and the reference electrodes, respectively. The indium tin oxide (ITO) coated glass with a sheet resistance of < 10 $\Omega \cdot sq^{-1}$ was used as working electrode. Before use, the ITO electrodes were cleaned by sonication successively in 0.5 M

Journal of Materials Chemistry A Accepted Manuscript

KOH and acetone for 10 and 15 min. The double-potential-step electrodeposition was performed at -0.400 V and 0.250 V *vs.* SCE for 20 ms and 0.5 h, respectively, in an aqueous solution of 0.2 M KNO_3, 5 mM $AgNO_3$ and 1 mM sodium citrate.

2.2 Preparation of the Ag/Ag_3PO_4 composite

The as-fabricated Ag NPs on the ITO substrate were used to prepare Ag/Ag_3PO_4 composite electrodes. After rinsed by high purity water, the Ag NP array electrodes were biased at 0.600 V *vs.* SCE for required time in 0.2 M Na_3PO_4 solution. The applied potential of 0.600 V *vs.* SCE is positive enough to oxidize surface Ag to Ag_3PO_4 in phosphate solution. The deposition of Ag_3PO_4 on the surface of Ag NPs was also illustrated in Fig. 1.

2.3 Characterization

The morphology of the Ag NPs and the Ag/Ag_3PO_4 composite were characterized by a field emission scanning electron microscope (FE-SEM, Hitachi S-4800) operating at an accelerate voltage of 10.0 kV. The transmission electron microscope (TEM) and selected area electron diffraction (SEAD) measurements were carried out on a field emission JEM-2010F microscope (JEOL Ltd., Japan) with an accelerate voltage of 200 kV. To prepare TEM samples, the Ag/Ag_3PO_4 composite nanoplates were scraped off from the ITO substrate and dispersed in ethanol under ultra-sonication, and the resulting ethanol solution was drop-casted on to the TEM grid and dried in air. The crystal structure of the Ag and Ag/Ag_3PO_4 composite was characterized by X-ray diffraction (XRD), which was performed on a Rigaku, rint2000 advance theta-2theta powder diffractometer with Cu Kα.. The height of the Ag NPs was characterized by tapping-mode atomic force microscopy (AFM, Multimode NanoScope IIIa, Veeco Instruments, USA).

Journal of Materials Chemistry A Accepted Manuscript

2.4 Photoelectrochemical measurements

All PEC measurements were carried out in a three-electrode PEC cell in a buffer solution of 0.2 M KH_2PO_4/K_2HPO_4 (pH = 7.0) with the Ag/Ag_3PO_4 composite as working electrode. A 300W xenon lamp was used as the light source and the incident light intensity on the electrode surface was 100 $mW \cdot cm^{-2}$. For all measurements under chopped illumination, a chopper was used to provide a chopped light beam with a required on/off duration. The electrochemical impedance spectroscopic (EIS) measurements were performed at a bias potential of 0.500 V *vs.* SCE in 0.2 M KH_2PO_4/K_2HPO_4 buffer solution (pH = 7.0) using a 10 mV amplitude perturbation between 100 kHz and 1 Hz.

2.5 Detection of oxygen evolution

Oxygen evolution was monitored using a fluorescence-based oxygen sensor (NeoFox, Ocean Optics FOSPOR-R, SN1217096). For the detection of oxygen evolution, a gas-tight three-compartment photoelectrochemical cell was used, with each compartment containing one electrode (the working, reference and counter electrodes). The light source was projected to the photoanode through a quartz window and the incident light intensity on the electrode surface was 100 $mW \cdot cm^{-2}$. A constant bias potential of 0.500 V *vs.* SCE was applied to the Ag/Ag_3PO_4 composite photoanode in 0.2 M KH_2PO_4/K_2HPO_4 (pH = 7.0) buffer solution. The oxygen sensor gave the volume percentage of oxygen *x%* in the headspace of the compartment that contained the Ag/Ag_3PO_4 composite photoanode. Hence, the mole quantity of O_2 evolution could be calculated using the Ideal Gas Equation: $pV = nRT$, where p is the air pressure, n is the mole quantity of O_2, R is the molar gas constant, T is the temperature, and V is the partial volume of oxygen. The value of V could be calculated from the headspace

Journal of Materials Chemistry A Accepted Manuscript

volume V^0 (175 ml) multiplied by *x*%. Prior to each measurement, the Ag/Ag_3PO_4 composite photoanode was first bias at 0.5 V under illumination for 5 min to reach a stable state, and then the photoelectrochemical cell was purged with high purity N_2 for 1 h to remove O_2 both in the solution and in the gas phase, and then the system was sealed and left static for 10 min to examine leakage.

3. Results and discussion.

3.1 The preparation and characterization of vertically aligned Ag NPs

Vertically aligned Ag NP arrays were deposited onto an ITO substrate by a two-step electrodeposition method, which consisted of a pulse potential step performed at -0.400 V *vs.* SCE for 20 ms and a normal potential step performed at 0.250 V *vs.* SCE for 0.5 h. The first, more negative pulse potential step provided a high cathodic overpotential to generate Ag nanoseeds, while the subsequent positive and longer deposition step provided a mild overpotential to grow Ag NPs.[36, 37] Fig. 2a shows a typical low-magnification SEM image of the as-prepared Ag NPs, which demonstrates that the NPs grow uniformly in large scale on the substrate. The high-magnification SEM image (Fig. 2b) indicates that most of the Ag NPs are interconnected to each other and perpendicularly oriented to the ITO surface. Statistic analysis of SEM images reveals that Ag NPs have an average thickness of *ca.* 25 nm and a width of *ca.* 2 μm.Fig. 2c shows the typical high-resolution TEM image of an Ag NP, from which the lattice spacing was obtained to be 0.249 nm, corresponding to the 3×{422} face-centred-cubic (fcc) lattice fringe that is associated with 1/3{422} diffraction shown in the SAED pattern (Fig. 2d) [38]. The 1/3{422} diffraction is normally forbidden for a defect-free

Journal of Materials Chemistry A Accepted Manuscript

fcc lattice and its appearance was attributed to the {111} stacking faults, which was crucial to the formation of Ag NPs [38]. The XRD pattern of Ag NPs is shown in Fig. 3, from which four diffraction peaks of fcc Ag (JCPDS 65-2871) and the diffraction peaks of ITO substrate were clearly identified. The four diffraction peaks of Ag appear at 38.18 °, 44.48 °, 64.60 ° and 77.54 °, which were indexed to (111), (200), (220) and (311) planes of fcc Ag, respectively. These results indicate that each Ag NP is a single crystal with the planar surface parallel to {111}. As is well known, AFM is highly sensitive to the height of surface features and it was used here to provide height information about the Ag NPs (Fig. S1 in the supplementary information). AFM cross-section analysis indicates that the height of Ag NPs varies from ca. 300 to 600 nm. It should be pointed out here that the obtained AFM height of the standing Ag NPs is a little smaller than its true height because it is difficult for the commercial AFM tip with a typical curvature radius of ca. 10 nm to reach the ITO substrate when imaging a closely packed NP structure. The obtained Ag NPs layer adhered tightly to the ITO substrate and was difficult to be removed from the substrate even by ultra-sonication in ethanol and water. This ensures not only an excellent adhesion but also a good electrical contact between the Ag NPs and the ITO substrate, both of which was very important when Ag NPs were used as electrode.

3.2 The preparation and characterization of the Ag/Ag_3PO_4 composite nanoplates

The vertically aligned Ag NPs constitutes an interconnected network that has a large specific area, a good conductivity and a strong adhesion to the ITO substrate. These features ensure the Ag NPs array an ideal framework for preparing Ag/Ag_3PO_4 composite NPs. Fig. 4a

Journal of Materials Chemistry A Accepted Manuscript

shows an anodic potential sweep curve of the Ag NPs electrode in the 0.2 M Na_3PO_4 solution, which exhibits the characteristics of a metal passivation process [39], indicating that Ag surface was coated with a blocking layer. As is well known, Ag can be oxidized to Ag_3PO_4 in phosphate solution according to the following equation:

$$3Ag - 3e^- + PO_4^{3-} \rightarrow Ag_3PO_4 \quad (1)$$

The standard potential of this reaction is 0.241 V *vs.* SCE (0.483 V *vs*. NHE), based on the standard potential of the Ag^+/Ag redox couple (0.799 V *vs.* NHE) and the K_{sp} of Ag_3PO_4 (8.89×10^{-17}) [30], and the equilibrium potential of Ag_3PO_4/Ag redox couple in 0.2 M Na_3PO_4 was calculated to be 0.255 V *vs.* SCE according to the Nernst equation. Therefore, the anodic peak in the potential range from 0.200 V to 0.500 V *vs*. SCE in Fig. 4a corresponds to the oxidation of Ag to Ag_3PO_4. The anodic current decreases sharply after it reaches the peak value at 0.380 V *vs.* SCE, indicating that the exposed Ag surface decreases greatly with the increase of potential. Fig. 4a also clearly shows a stable passive region from ca. 0.5 V to 0.7 V *vs.* SCE, within which a very small anodic current was observed, suggesting that nearly all Ag surface was blocked by the Ag_3PO_4 layer.

Based on this result, the Ag/Ag_3PO_4 composite was fabricated by electro-oxidation of surface Ag in 0.2 M Na_3PO_4 at a constant potential of 0.600 V *vs.* SCE. The corresponding current-time response was presented in Fig. 4b, which shows an abrupt decrease in the initial 20 s and a slow decrease to nearly zero in about 60 s. This result indicates that the majority of Ag surface was coated with Ag_3PO_4 in 20 s and nearly all Ag surface was blocked by Ag_3PO_4 within 60 s. The Ag_3PO_4 blocking layer acted as a protection shield against the further oxidation of the inner Ag. The charge consumed to oxidize surface Ag within 60 s can be

Journal of Materials Chemistry A Accepted Manuscript

obtained by integrating the current-time curve shown in Fig. 4b, and the obtained value was 0.060 $C \cdot cm^{-2}$, which is only *ca.* 7% of the charge used to prepare Ag NPs (0.847 $C \cdot cm^{-2}$, see Fig. 4c). This result confirms that only the surface Ag was converted to Ag_3PO_4 and the inner Ag remains intact.

A typical SEM image of the Ag/Ag_3PO_4 composite with an oxidation time of 8 s is shown in Fig. 5a, which demonstrates that the Ag NPs were coated with an Ag_3PO_4 layer and the vertically-oriented NP structure remained almost unchanged after electro-oxidation. Energy dispersive spectrum (EDS) of the Ag/Ag_3PO_4 composite show the peaks of Ag, P and O (Fig. S2), providing indirect evidence of the formation of Ag_3PO_4 on the surface of Ag NPs. Fig. 5b shows the high-resolution TEM image of the Ag/Ag_3PO_4 composite, in which both the lattice spacing of the fcc Ag (111) planes (d = 0.236 nm) and the lattice spacing of the body-centred cubic (bcc) Ag_3PO_4 (210) planes (d = 0.268 nm) are observed, suggesting the coexistence of Ag and Ag_3PO_4. The XRD pattern of the Ag/Ag_3PO_4 composite was shown in Fig. 3. The diffraction peaks of Ag_3PO_4 appear at 38.13°, 44.30°, *etc*., which can be indexed to the (210) , (211) and other planes of bcc Ag_3PO_4 (JCPDS 6-505) [21]. Besides, four peaks of fcc Ag (JCPDS 65-2871) were still clearly seen, indicating that large amount of zero-valent Ag exists beneath the Ag_3PO_4 coating layer.

All these results provide solid evidence that an Ag_3PO_4 layer was successfully produced on the surface of Ag NPs by electrooxidation in phosphate solution, forming a vertically aligned Ag/Ag_3PO_4 composite NP array. The generated surface Ag_3PO_4 acts as a passivation layer, protecting the inner Ag from further oxidation. Moreover, the deposited amount of Ag_3PO_4 can be easily tuned by controlling the electrooxidation time (see Fig. S3 in the

Journal of Materials Chemistry A Accepted Manuscript

supplementary information).

3.3 The activity of the Ag/Ag_3PO_4 composite for PEC OER

The aligned nanostructures composed of one- or two-dimensional semiconductors ensure a large specific area, which benefits not only the light absorption property but also the photoactivity [17, 18, 23, 40]. Herein, the Ag/Ag_3PO_4 composite NPs were employed as photoanode for PEC OER. Fig. 6a shows the linear potential sweep voltammograms of Ag/Ag_3PO_4 photoanode in 0.2 M KH_2PO_4/K_2HPO_4 buffer solution (pH = 7.0) in the dark and under 100 mW/cm^2 illumination. Because the Ag/Ag_3PO_4 composite photoanode used in Fig. 6a were prepared at 0.600 V *vs.* SCE with only 8 s of Ag_3PO_4 deposition time, large surface areas of Ag NPs were not coated with Ag_3PO_4. As a result, the Ag/Ag_3PO_4 composite exhibited a dark current during the potential sweep, which arose from the electrooxidation of the exposed Ag surface. When illuminated, the Ag/Ag_3PO_4 composite showed a large photocurrent density that was attributed to both the OER and the oxidation of surface Ag to Ag_3PO_4 [8]. The percentage of the photocurrent for OER can be evaluated by monitoring the amount of evolved O_2, and the results will be discussed later.

The thickness of the Ag_3PO_4 layer, which is determined by the Ag_3PO_4 deposition time, has an important effect on the photocatalytic activity of Ag/Ag_3PO_4 photoanode. Fig. 6b shows the influence of the Ag_3PO_4 deposition time on the linear potential sweep voltammograms of the Ag/Ag_3PO_4 composite. To simultaneously present both the photocurrent and the dark current, a chopped light was employed as illumination source. The dark current densities gradually decreases as the deposition time increases, which confirms

Journal of Materials Chemistry A Accepted Manuscript

that the dark current corresponds to the oxidation of the exposed Ag NP surface. The photocurrent densities (the difference between light and dark current densities) of different Ag/Ag_3PO_4 samples were quite similar in value in the high potential range (> 0.600 V *vs.* SCE) (Fig. 6b). However, in the low potential range (< 0.600 V *vs.* SCE), the photocurrent greatly depended on the Ag_3PO_4 deposition time. We found that the composite photoanode with a deposition time of 8 s exhibited high activity and relative low dark current especially at low overpotentials. We believe this observation is due to the balance between the increase of light absorption property and the decrease of conductivity of Ag_3PO_4 with increasing the Ag_3PO_4 layer thickness.

Considering that the applied potential is in fact a power input, the improvement of photocatalytic activity in low potential range is of great significance. To reduce the external power input, all constant potential PEC measurements were performed at a bias of 0.500 V *vs.* SCE, which is lower than the redox potential of O_2/H_2O couple at pH = 7.0, ensuring that no electrooxidation of water occurs. Fig. 6c shows the current-time responses at a bias of 0.500 V *vs.* SCE under chopped illumination using the composite photoanodes prepared with different Ag_3PO_4 deposition time. From Fig. 6c it is seen that, the photocurrent decreases with increasing Ag_3PO_4 deposition time. Moreover, a stable photocurrent can be obtained only when the Ag_3PO_4 deposition time exceeds 8 s. Fig. 6c clearly shows that the composite with 8 s Ag_3PO_4 deposition time exhibits a high and stable photocurrent density of ca. 0.25 $mA \cdot cm^{-2}$. This value is the highest among those previously reported on Ag_3PO_4-related photoanodes [9, 14, 28]. Therefore, the Ag/Ag_3PO_4 samples with 8 s Ag_3PO_4 deposition time were employed for all other PEC measurements including EIS and oxygen evolution rate measurements

Journal of Materials Chemistry A Accepted Manuscript

discussed later.

The electrochemical impedance spectroscopy (EIS) was also used to evaluate the photoactivity of the Ag/Ag_3PO_4 composite. Fig. 7 shows EIS spectra of the composite photoanode at a constant bias of 0.500 V *vs.* SCE in the dark and under illumination. Both the EIS spectra showed two impedance semicircles, with the high frequency semicircle reflecting the contact resistance and capacitance at the Ag/ITO interface. As the EIS data were obtained at 0.500 V *vs.* SCE, which was much lower than the oxygen-evolution potential (0.574 V *vs.* SCE) at pH = 7, the only possible charge transfer reaction is the oxidation of surface Ag. Accordingly, the diameter of the low frequency semicircle in the dark reflects the resistance of the electrooxidation of Ag to Ag_3PO_4. When the photoanode was illuminated, the diameter of the low frequency semicircle decreases to half of its original value, suggesting that the illumination facilitates the charge transfer reactions at the Ag/Ag_3PO_4/solution interfaces. Herein, the photoinduced holes may get involved in both the OER and the oxidation of Ag due to their high oxidizing capability. So, there remains a question as which of the following two reactions, the PEC oxidation of Ag or the PEC OER contributes more to the improvement of charge transfer rate under illumination. To answer this question, it is necessary to monitor the oxygen evolution rate during PEC OER.

3.4 The oxygen evolution rate at the Ag/Ag_3PO_4 composite photoanode during PEC OER

To investigate whether the photocurrent mainly comes from OER or from the oxidation of Ag, we used a gas-tight PEC cell to detect the evolution of oxygen at a bias of 0.500 V *vs.* SCE in KH_2PO_4/K_2HPO_4 buffer solution (pH = 7.0). According to the Nernst Equation, the

Journal of Materials Chemistry A Accepted Manuscript

equilibrium potential of the O_2/H_2O redox couple in an electrolyte at pH = 7.0 is 0.574 V *vs.* SCE. So under the bias of 0.500 V *vs.* SCE, the electrochemical OER cannot occur. This makes sure that all evolved O_2 comes from PEC OER.

We firstly biased the Ag/Ag_3PO_4 composite photoanodes (with Ag_3PO_4 deposition time of 8 s and 60 s, and denoted as the Ag/Ag_3PO_4 (8 s) and the Ag/Ag_3PO_4 (60 s) photoanodes, respectively) at a constant potential of 0.500 V *vs.* SCE in the dark, and no O_2 evolution was detected. However, when illuminated, both photoanodes evolved O_2, as shown in Fig. 8. There is a time lag for the onset of O_2 signal, and this is due to the following two reasons. (1) The whole cell was deoxygenated with N_2, and (2) the oxygen sensor was placed in the headspace of the cell and it took time for the evolved O_2 to first dissolve in solution and then diffuse into the gas phase. After the expected initial lag, the detected O_2 production rate agrees well with the theoretical one that was calculated by integrating the photocurrent and assuming the photocurrent arises from the 4-electron-involved OER. The detected-O_2-production-rate obtained at the Ag/Ag_3PO_4 (8 s) photoanode is 2.15×10^{-3} μmol·s^{-1} (Fig. 8a), which is a little smaller than the calculated one of 2.25×10^{-3} μmol·s^{-1}. The Faraday efficiency (η_F) of OER at Ag/Ag_3PO_4 (8 s) photoanode can be estimated by the ratio of the detected- to calculated-O_2-production-rate. The obtained value of η_F in Fig. 8a is 95.6%, which suggests that most of the photocurrent were engaged in OER. While for the Ag/Ag_3PO_4 (60 s) photoanode, the detected-O_2-production-rate and the calculated-O_2-production-rate are 7.65×10^{-4} μmol·s^{-1} and 8.65×10^{-4} μmol·s^{-1}, respectively, resulting in an η_F value of 87.3%, which is a little smaller than that of Ag/Ag_3PO_4 (8 s) photoanode. The oxygen evolution

Journal of Materials Chemistry A Accepted Manuscript

results provide solid evidence that the PEC OER contributes most to the photocurrent, making the Ag/Ag_3PO_4 composite an efficient photoanode for PEC OER.

It should be pointed out that, the other 4.4 % and 12.7% photocurrents at the Ag/Ag_3PO_4 (8 s) and the Ag/Ag_3PO_4 (60 s) photoanodes, respectively, were consumed to oxidize the surface Ag to Ag_3PO_4. This part of photocurrent is very important to the long-term stability of the Ag/Ag_3PO_4 photoanodes. As is known, Ag_3PO_4 may decompose or dissolve slightly into the solution [14, 25-27], resulting in a fast decay of its photoactivity. The *in situ* oxidation of surface Ag in phosphate solution can make up for the loss of Ag_3PO_4 during PEC OER. Therefore, the Ag/Ag_3PO_4 composite works as a self-healing system in phosphate solution, and then improves the stability of the photoanode. Contrast PEC OER experiments was conducted in a PO_4^{3-} absent electrolyte, for example Na_2SO_4 or $NaNO_3$ solution, a great decrease of photocurrent with time was observed, implying the significance of the self-healing mechanism for the Ag/Ag_3PO_4 composite photoanode. The long-term stability of the Ag/Ag_3PO_4 (8 s) photoelectrode was tested under chopped illumination (with the on/off duration of 1 min/1 min) for 1 h. The current density-time response of the composite electrode at 0.500 V *vs.* SCE was shown in Fig. 9a. The photocurrent density decreased from ca. 0.29 $mA \cdot cm^{-2}$ to ca. 0.19 $mA \cdot cm^{-2}$ in the first 10 min, and then decreased slowly in the next 50 min to ca. 0.10 $mA \cdot cm^{-2}$, showing a decay to 34% of the original value. Fig. 9b shows the XRD spectra of the composite photoanode before and after the 1 h reaction. The XRD patterns of both bcc Ag_3PO_4 and fcc Ag were observed after 1 h measurement, suggesting the composition of the composite photoanode remains stable.

3.5 Mechanism of the Ag/Ag_3PO_4 composite as efficient photoanode for OER

Journal of Materials Chemistry A Accepted Manuscript

Fig. 10 shows the band structure and the charge transfer mechanism at the Ag/Ag_3PO_4/electrolyte interfaces. As shown in Fig. 10a, the conduction and valence band edges of Ag_3PO_4 are located at 0.44 V and 2.89 V *vs.* NHE, respectively [8]. As is well known, when a semiconductor is contact with an electrolyte solution, a space charge region is formed and the potential of space charge region leads to band bending inside the semiconductor. For a n-type semiconductor such as Ag_3PO_4, the bands are bent upward with respect to the energy level in the bulk semiconductor. Therefore the potential of space charge region inside Ag_3PO_4 separate the photoinduced electron-hole pairs by driving the holes to the Ag_3PO_4/solution interface and the electrons to the bulk of Ag_3PO_4. As the position of the band at the semiconductor/solution interface does not change, the photoinduced holes have enough energy to oxidize water because the equilibrium OER potential (0.816 V *vs.* NHE) at pH = 7.0 is much lower than the valence band edge of Ag_3PO_4 (2.89 V *vs.* NHE). The Fermi level of Ag NPs is determined by the externally applied potential. When the Ag/Ag_3PO_4 composite was biased at a potential higher than 0.44 V *vs.* NHE (corresponding to 0.20 V *vs.* SCE), the photoinduced electrons can be, in principle, injected into Ag NPs from the conduction band of Ag_3PO_4, thus completing the electron-hole separation. The photoinduced holes at Ag_3PO_4/solution interface will be captured by water or Ag, resulting in the oxidation of water or the formation of Ag_3PO_4 on the Ag NP surface. According to the results of oxygen evolving measurements, most of the separated photoinduced holes (95.6% at the Ag/Ag_3PO_4 (8 s) photoanode and 87.3% at the Ag/Ag_3PO_4 (60 s) photoanode) were involved in water oxidation, and the rest were involved in the oxidation of Ag to Ag_3PO_4. The latter process ensures the Ag/Ag_3PO_4 composite a self-healing system in phosphate solution.

Journal of Materials Chemistry A Accepted Manuscript

Fig. 10b illustrates the function of the vertically-aligned Ag NPs during PEC OER. The Ag NPs act both as a framework to support Ag_3PO_4 and as an electron collector. As is known, with the consumption of holes in OER, the photoinduced electrons accumulate in Ag_3PO_4 if they are not efficiently drained off to the counter electrode. The accumulation of electrons can result in electron-hole recombination and reductive decomposition of Ag_3PO_4,[8, 27] and then lowers the activity and stability of the composite photoanode. While in this work, due to the excellent conductivity of Ag, the Ag NP framework greatly facilitates electron transport from Ag_3PO_4 to counter electrode with the help of applied bias, and then significantly improves the PEC activity and stability of the photoanode by decreasing electron accumulation in Ag_3PO_4.

4. Conclusion

In summary, we report a facile way to fabricate the vertically aligned Ag/Ag_3PO_4 composite NPs, which exhibit high activity and stability toward PEC water oxidation. The photocurrent density of the Ag/Ag_3PO_4 composite photoanode at 0.500 V *vs.* SCE reached 0.25 $mA \cdot cm^{-2}$, and the Faraday efficiency for OER was 95.6%, indicating that most of the photocurrent was involved in PEC OER. The excellent performance of the composite photoanodes for PEC OER is due to the following three reasons. (1) The aligned NP structure provides a large specific area that benefits not only the light absorption but also the charge transfer reaction occurred at Ag_3PO_4/solution interfaces. (2) The excellent conductivity of Ag NPs facilitates electron-hole separation inside the composite and then improves the activity of photoanode toward PEC OER. (3) The self-healing mechanism of the composite in phosphate solution greatly enhances its stability during OER. This work may provide insights into the

Journal of Materials Chemistry A Accepted Manuscript

rational design and construction of a nanoscaled conductor/semiconductor composite structure for efficient photo-to-chemical conversion.

Acknowledgements

We gratefully acknowledge the financial support of this work by National Natural Science Foundation of China (NSFC 21173016), Beijing Natural Science Foundation (2142020 and 2151001).

Reference

[1] M.G. Walter, E.L. Warren, J.R. McKone, S.W. Boettcher, Q. Mi, E.A. Santori, N.S. Lewis, Chem. Rev. 110 (2010) 6446-6473.

[2] P.V. Kamat, J. Phys. Chem. C 111 (2007) 2834-2860.

[3] T. Hisatomi, J. Kubota, K. Domen, Chem. Soc. Rev. 43 (2014) 7520-7535.

[4] J. Sun, D.K. Zhong, D.R. Gamelin, Energy Environ. Sci. 3 (2010) 1252-1261.

[5] A. Fujishima, K. Honda, Nature 238 (1972) 37-38.

[6] J.K. Hurst, Science 328 (2010) 315-316.

[7] M. Gratzel, Nature 414 (2001) 338-344.

[8] Z. Yi, J. Ye, N. Kikugawa, T. Kako, S. Ouyang, H. Stuart-Williams, H. Yang, J. Cao, W. Luo, Z. Li, Y. Liu, R.L. Withers, Nat. Mater. 9 (2010) 559-564.

[9] Y. Hou, F. Zuo, Q. Ma, C. Wang, L. Bartels, P. Feng, J. Phys. Chem. C 116 (2012) 20132-20139.

[10] X. Yang, H. Cui, Y. Li, J. Qin, R. Zhang, H. Tang, ACS Catal. 3 (2013) 363-369.

[11] J. Ma, J. Zou, L. Li, C. Yao, T. Zhang, D. Li, Appl. Catal. B-Environ. 134 (2013) 1-6.

Journal of Materials Chemistry A Accepted Manuscript

[12] J. Wang, F. Teng, M. Chen, J. Xu, Y. Song, X. Zhou, CrystEngComm 15 (2013) 39-42.

[13] B. Zheng, X. Wang, C. Liu, K. Tan, Z. Xie, L. Zheng, J. Mater. Chem. A 1 (2013) 12635-12640.

[14] Y. Bi, S. Ouyang, J. Cao, J. Ye, Phys. Chem. Chem. Phys. 13 (2011) 10071-10075.

[15] D.C.a.J.M. G. Hodes, Nature 260 (1976) 312–313.

[16] D.-D. Qin, C.-L. Tao, S.A. Friesen, T.-H. Wang, O.K. Varghese, N.-Z. Bao, Z.-Y. Yang, T.E. Mallouk, C.A. Grimes, Chem. Commun. 48 (2012) 729-731.

[17] T. Jin, P. Diao, D. Xu, Q. Wu, Electrochim. Acta 114 (2013) 271-277.

[18] T. Jin, P. Diao, Q. Wu, D. Xu, D. Hu, Y. Xie, M. Zhang, Appl. Catal. B: Environ. 148-149 (2014) 304-310.

[19] N. Aiga, Q. Jia, K. Watanabe, A. Kudo, T. Sugimoto, Y. Matsumoto, J. Phys. Chem. C 117 (2013) 9881-9886.

[20] D.K. Zhong, S. Choi, D.R. Gamelin, J. Am. Chem. Soc. 133 (2011) 18370-18377.

[21] Y. Bi, H. Hu, S. Ouyang, Z. Jiao, G. Lu, J. Ye, J. Mater. Chem. 22 (2012) 14847-14850.

[22] V. Subramanian, E.E. Wolf, P.V. Kamat, J. Phys. Chem. B 107 (2003) 7479-7485.

[23] J. Shi, Y. Hara, C. Sun, M.A. Anderson, X. Wang, Nano Lett. 11 (2011) 3413-3419.

[24] D. Wang, X. Zhang, P. Sun, S. Lu, L. Wang, C. Wang, Y. Liu, Electrochim. Acta 130 (2014) 290-295.

[25] Y. Liu, L. Fang, H. Lu, Y. Li, C. Hu, H. Yu, Applied Catalysis B: Environmental 115-116 (2012) 245-252.

[26] Y. Liu, L. Fang, H. Lu, L. Liu, H. Wang, C. Hu, Catal. Commun. 17 (2012) 200-204.

[27] H. Wang, Y. Bai, J. Yang, X. Lang, J. Li, L. Guo, Chem. Eur. J. 18 (2012) 5524-5529.

Journal of Materials Chemistry A Accepted Manuscript

[28] Y. Bi, H. Hu, S. Ouyang, G. Lu, J. Cao, J. Ye, Chem. Commun. 48 (2012) 3748-3750.

[29] W.-S. Wang, H. Du, R.-X. Wang, T. Wen, A.-W. Xu, Nanoscale 5 (2013) 3315-3321.

[30] J.A. Dean, Lange's Handbook of Chemistry, 15th ed., McGraw-Hill, Inc., New York, 1999.

[31] H. Zhang, H. Huang, H. Ming, H. Li, L. Zhang, Y. Liu, Z. Kang, J. Mater. Chem. 22 (2012) 10501-10506.

[32] L. Zhang, H. Zhang, H. Huang, Y. Liu, Z. Kang, New J. Chem. 36 (2012) 1541-1544.

[33] C.D. Grosh, D.T. Schwartz, F. Baneyx, Cryst. Growth Des. 9 (2009) 4401-4406.

[34] G. Liu, W. Cai, C. Liang, Cryst. Growth Des. 8 (2008) 2748-2752.

[35] C. Gu, T.Y. Zhang, Langmuir 24 (2008) 12010-12016.

[36] D. Xu, X. Yan, P. Diao, P. Yin, J. Phys. Chem. C 118 (2014) 9758-9768.

[37] Y. Li, P. Diao, T. Jin, J. Sun, D. Xu, Electrochim. Acta 83 (2012) 146-154.

[38] V. Germain, J. Li, D. Ingert, Z.L. Wang, M.P. Pileni, J. Phys. Chem. B 107 (2003) 8717-8720.

[39] Y.S. Zhang, X.M. Zhu, M. Liu, R.X. Che, Appl. Surf. Sci. 222 (2004) 89-101.

[40] J. Su, X. Feng, J.D. Sloppy, L. Guo, C.A. Grimes, Nano Lett. 11 (2010) 203-208.

Journal of Materials Chemistry A Accepted Manuscript

Figure Captions

Fig. 1. Schematic illustration of the preparation of the vertically aligned Ag NPs and the deposition of Ag_3PO_4 on the surface of Ag NPs. The electrodeposition was carried out in a three-electrode cell and only the working and counter electrodes were illustrated here for brevity.

Fig. 2. (a) low magnification and (b) high magnification SEM images of Ag NPs. (c) high-resolution TEM image and (d) SAED pattern of Ag NPs.

Fig. 3. XRD patterns of the Ag NPs (red) and the Ag/Ag_3PO_4 composite (blue).

Fig. 4. (a) The linear potential sweep voltammogram of the Ag NPs electrode in 0.2 M Na_3PO_4. (b) The current density-time response of the Ag NPs electrode during the Ag_3PO_4 deposition procedure, in which the surface Ag was oxidized to Ag_3PO_4 at an anodic bias of 0.600 V *vs.* SCE in 0.2 M Na_3PO_4. The blue area under current line represents the integrated charge involved in the oxidation of Ag. (c) The current density-time curve during the deposition of Ag NPs on ITO substrate at a cathodic bias of 0.250 V *vs.* SCE in an aqueous solution of 0.2 M KNO_3, 5 mM $AgNO_3$ and 1 mM sodium citrate. The blue area under current line represents the integrated charge involved in the reduction of Ag^+ to Ag.

Fig. 5. (a) SEM and (b) high-resolution TEM images of Ag/Ag_3PO_4 composite, which was prepared with 8 s Ag_3PO_4 deposition time.

Fig. 6. (a) Linear potential sweep voltammograms of the Ag/Ag_3PO_4 composite photoanode in the dark and under illumination at a scan rate of 10 $mV \cdot s^{-1}$. The Ag_3PO_4 deposition time of the the Ag/Ag_3PO_4 composite photoanode is 8 s. (b) The linear potential sweep responses of different Ag/Ag_3PO_4 composite photoanodes under chopped illumination. (c) The current density-time response of the composite photoanode at 0.500 V *vs.* SCE under chopped illumination. All the photoelectrochemical tests were performed in 0.2 M KH_2PO_4/K_2HPO_4

Journal of Materials Chemistry A Accepted Manuscript

buffer solution (pH = 7.0) under 100 mW·cm^{-2} illumination. The Ag/Ag_3PO_4 composite photoanodes were prepared with Ag_3PO_4 deposition time of 4, 8, 16, 60 s.

Fig. 7. EIS spectra of the Ag/Ag_3PO_4 composite photoanode in the dark and under illumination. The EIS measurements were performed at a bias potential of 0.500 V *vs.* SCE in 0.2 M KH_2PO_4/K_2HPO_4 buffer solution (pH = 7.0) using a 10 mV amplitude perturbation between 100 kHz and 1 Hz.

Fig. 8. The calculated (open circles) and detected (solid circles) oxygen evolution on the Ag/Ag_3PO_4 composite photoanode with the Ag_3PO_4 deposition time of 8 s (a) and 60 s (b) at a constant bias of 0.500 V *vs.* SCE in 0.2 M KH_2PO_4/K_2HPO_4 buffer solution (pH =7.0) under 100 mW·cm^{-2} illumination.

Fig. 9. (a) long-term stability of the Ag/Ag_3PO_4 (8 s) composite photoanode. The test was performed at 0.500 V vs. SCE in 0.2 M KH_2PO_4/K_2HPO_4 buffer solution (pH = 7.0) under 100 mW·cm^{-2} illumination. (b)XRD patterns of the Ag/Ag_3PO_4 composite photoanode before and after 1 h PEC OER.

Fig. 10. Schematic illustrations for (a) the band structure and (b) the charge-flow diagram of the Ag/Ag_3PO_4 composite for PEC OER.

Journal of Materials Chemistry A Accepted Manuscript

Fig. 1

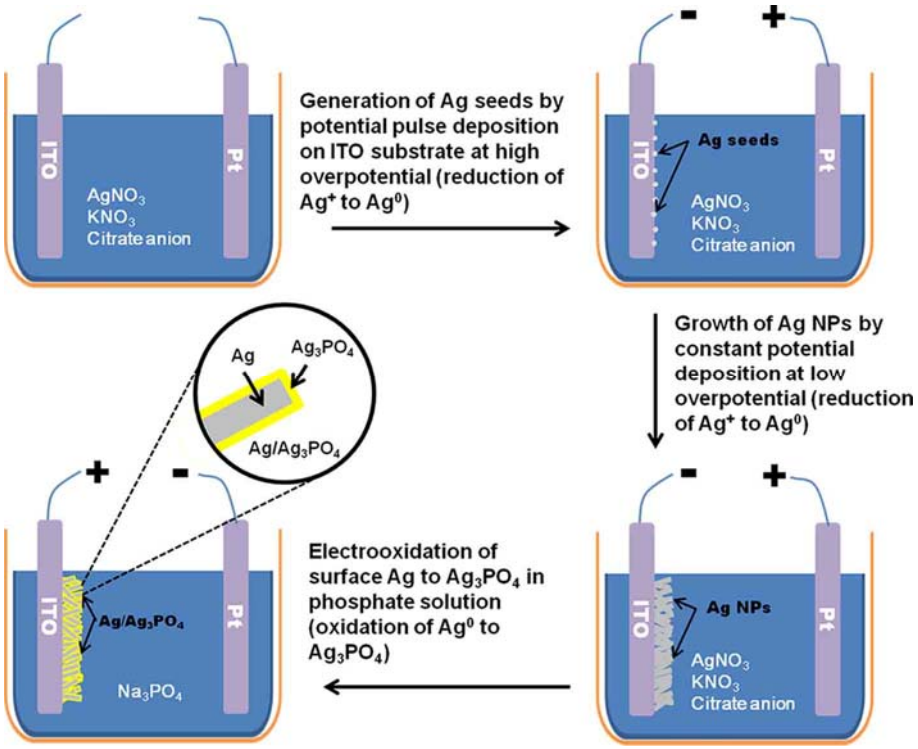

Fig. 1. Schematic illustration of the preparation of the vertically aligned Ag NPs and the deposition of Ag_3PO_4 on the surface of Ag NPs. The electrodeposition was carried out in a three-electrode cell and only the working and counter electrodes were illustrated here for brevity.

Journal of Materials Chemistry A Accepted Manuscript

Fig. 2

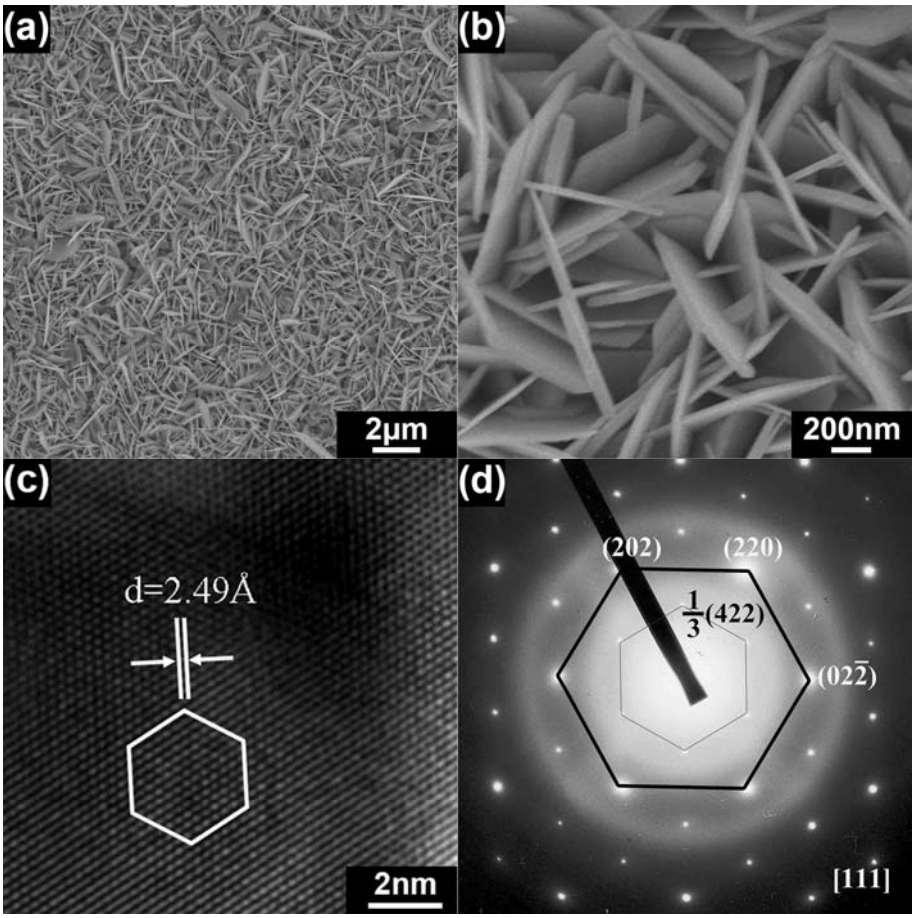

Fig. 2. (a) low magnification and (b) high magnification SEM images of Ag NPs. (c) high-resolution TEM image and (d) SAED pattern of Ag NPs.

Journal of Materials Chemistry A Accepted Manuscript

Fig. 3

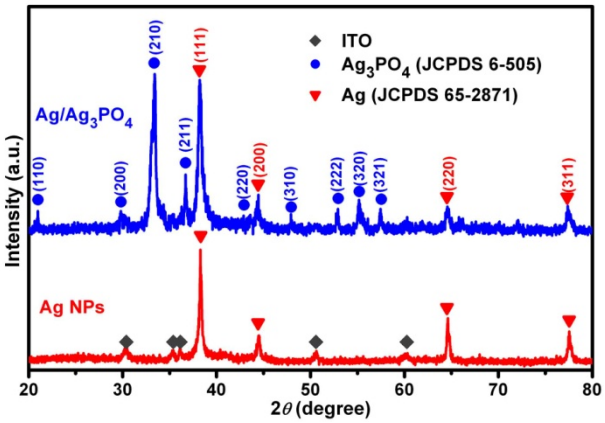

Fig. 3. XRD patterns of the Ag NPs (red) and the Ag/Ag_3PO_4 composite (blue).

Journal of Materials Chemistry A Accepted Manuscript

Fig. 4

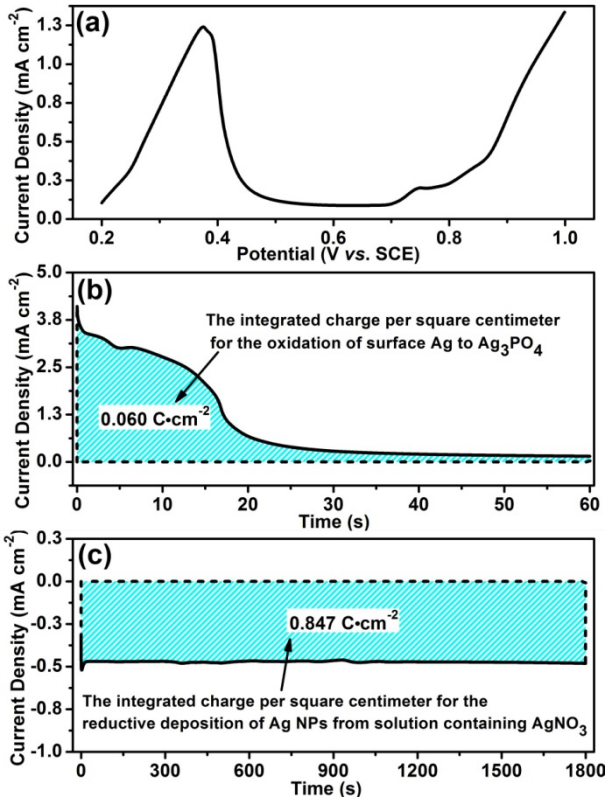

Fig. 4. (a) The linear potential sweep voltammogram of the Ag NPs electrode in 0.2 M Na_3PO_4. (b) The current density-time response of the Ag NPs electrode during the Ag_3PO_4 deposition procedure, in which the surface Ag was oxidized to Ag_3PO_4 at an anodic bias of 0.600 V *vs.* SCE in 0.2 M Na_3PO_4. The blue area under current line represents the integrated charge involved in the oxidation of Ag. (c) The current density-time curve during the deposition of Ag NPs on ITO substrate at a cathodic bias of 0.250 V *vs.* SCE in an aqueous solution of 0.2 M KNO_3, 5 mM $AgNO_3$ and 1 mM sodium citrate. The blue area under current line represents the integrated charge involved in the reduction of Ag^+ to Ag.

Journal of Materials Chemistry A Accepted Manuscript

Fig. 5

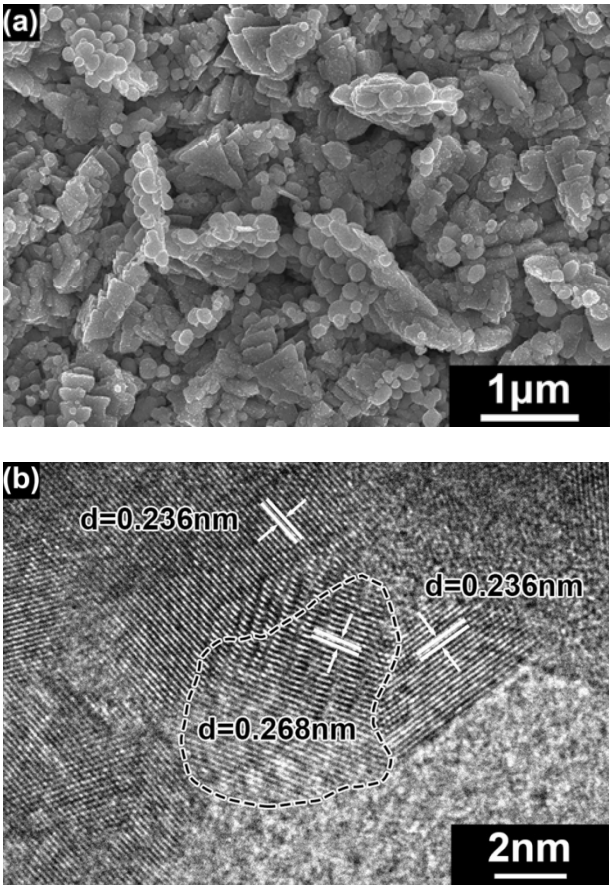

Fig. 5. (a) SEM and (b) high-resolution TEM images of Ag/Ag_3PO_4 composite, which was prepared with 8 s Ag_3PO_4 deposition time.

Journal of Materials Chemistry A Accepted Manuscript

Fig. 6

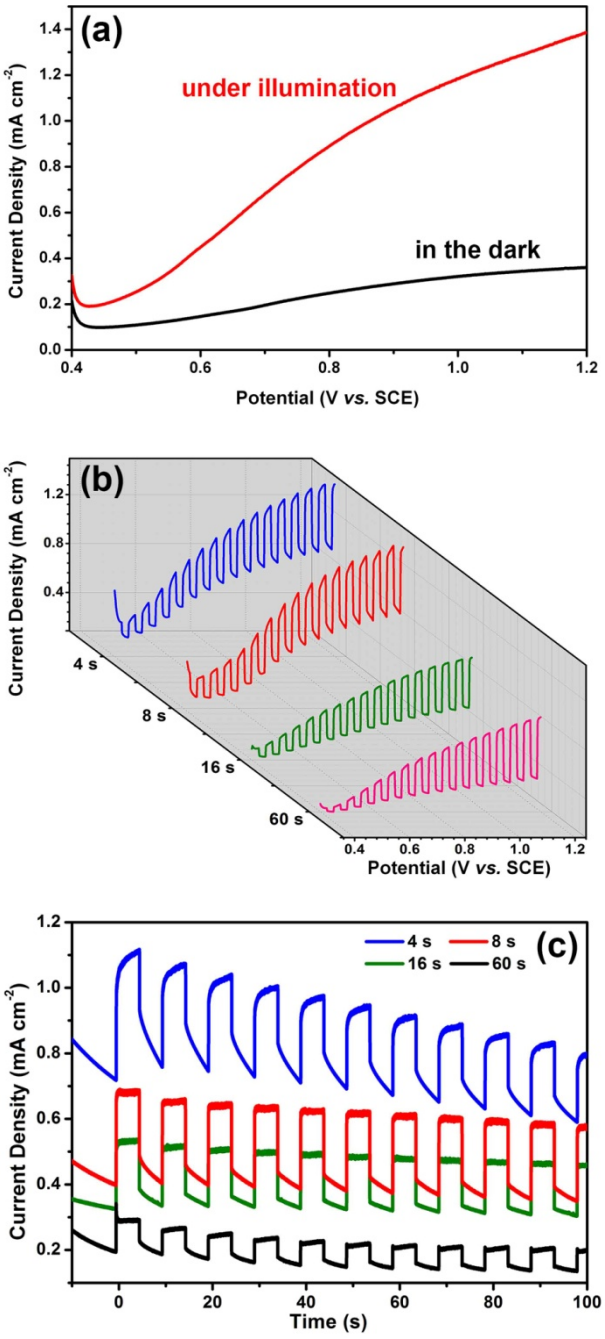

Fig. 6. (a) Linear potential sweep voltammograms of the Ag/Ag_3PO_4 composite photoanode in the dark and under illumination at a scan rate of 10 mV·s^{-1}. The Ag_3PO_4 deposition time of the the Ag/Ag_3PO_4 composite photoanode is 8 s. (b) The linear potential sweep responses of different Ag/Ag_3PO_4 composite photoanodes under chopped illumination. (c) The current density-time response of the composite photoanode at 0.500 V *vs.* SCE under chopped illumination. All the photoelectrochemical tests were performed in 0.2 M KH_2PO_4/K_2HPO_4 buffer solution (pH = 7.0) under 100 mW·cm^{-2} illumination. The Ag/Ag_3PO_4 composite photoanodes were prepared with Ag_3PO_4 deposition time of 4, 8, 16, 60 s.

Journal of Materials Chemistry A Accepted Manuscript

Fig. 7

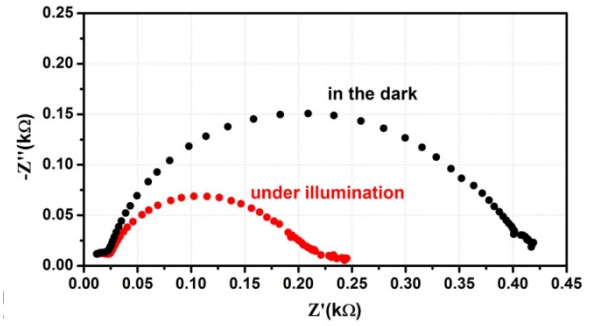

Fig. 7. EIS spectra of the Ag/Ag_3PO_4 composite photoanode in the dark and under illumination. The EIS measurements were performed at a bias potential of 0.500 V *vs.* SCE in 0.2 M KH_2PO_4/K_2HPO_4 buffer solution (pH = 7.0) using a 10 mV amplitude perturbation between 100 kHz and 1 Hz.

Journal of Materials Chemistry A Accepted Manuscript

Fig. 8

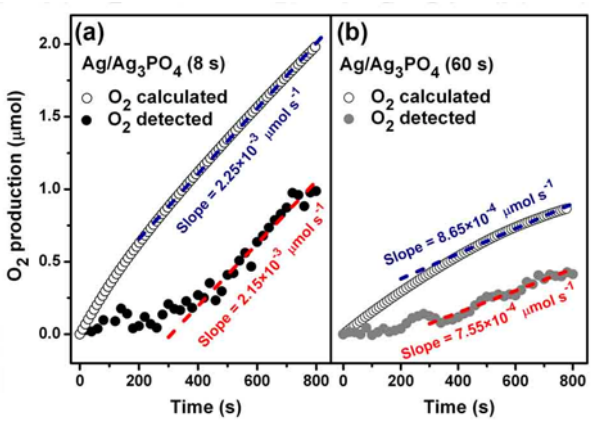

Fig. 8. The calculated (open circles) and detected (solid circles) oxygen evolution on the Ag/Ag_3PO_4 composite photoanode with the Ag_3PO_4 deposition time of 8 s (a) and 60 s (b) at a constant bias of 0.500 V *vs.* SCE in 0.2 M KH_2PO_4/K_2HPO_4 buffer solution (pH =7.0) under 100 $mW{\cdot}cm^{-2}$ illumination.

Journal of Materials Chemistry A Accepted Manuscript

Fig. 9

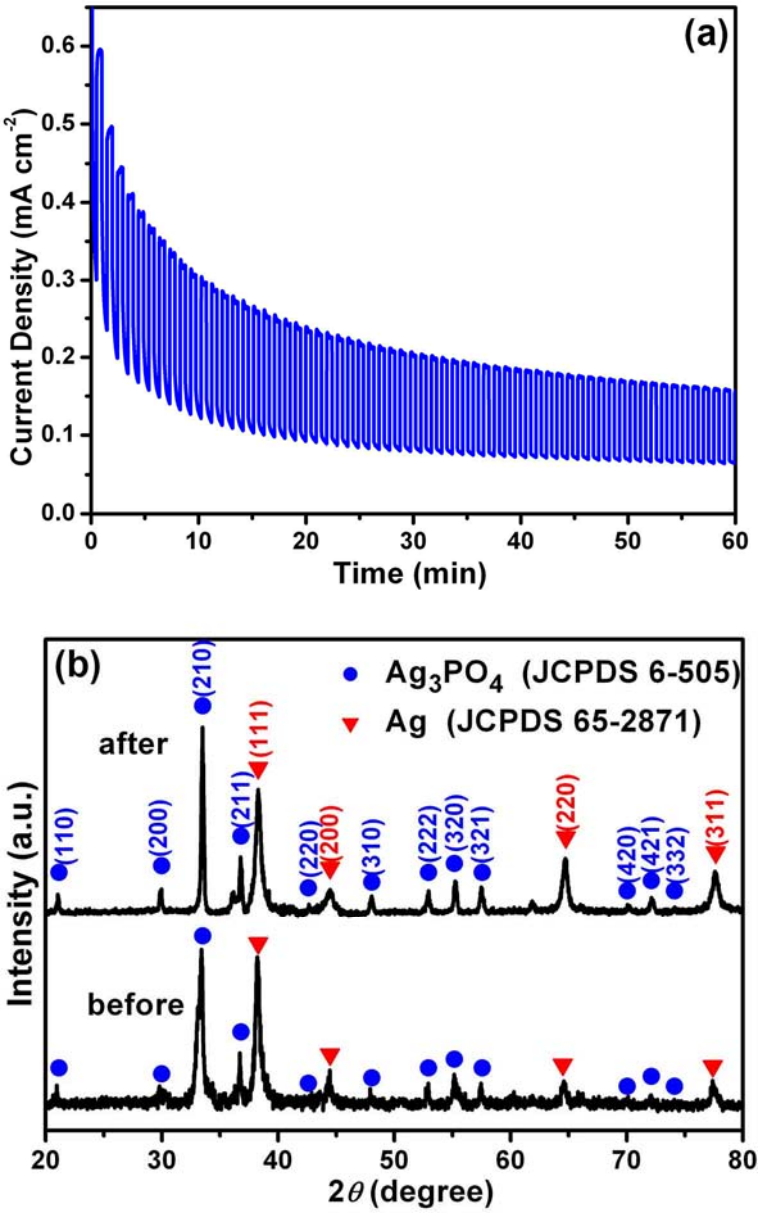

Fig. 9. (a) long-term stability of the Ag/Ag_3PO_4 (8 s) composite photoanode. The test was performed at 0.500 V vs. SCE in 0.2 M KH_2PO_4/K_2HPO_4 buffer solution (pH = 7.0) under 100 $mW{\cdot}cm^{-2}$ illumination. (b)XRD patterns of the Ag/Ag_3PO_4 composite photoanode before and after 1 h PEC OER.

Journal of Materials Chemistry A Accepted Manuscript

Fig. 10

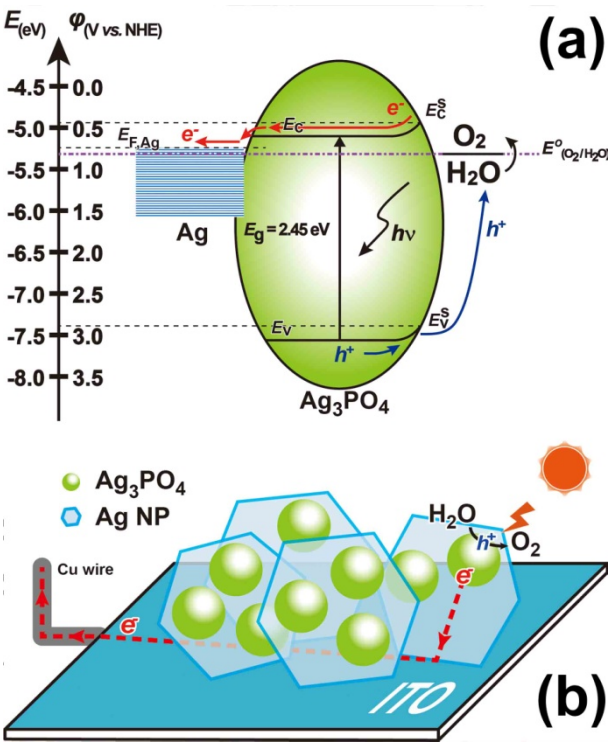

Fig. 10. Schematic illustrations for (a) the band structure and (b) the charge-flow diagram of the Ag/Ag_3PO_4 composite for PEC OER.

Journal of Materials Chemistry A Accepted Manuscript

Table of Contents (TOC):

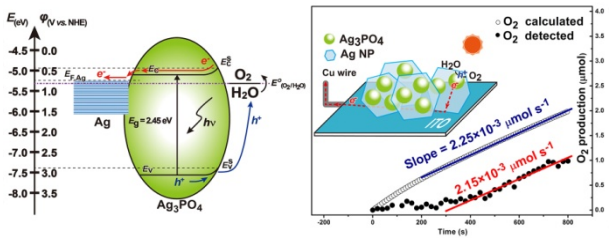

SYNOPSIS

The Ag/Ag_3PO_4 composite photoanode based on vertically-aligned Ag nanoplates exhibited high activity and stability toward photoelectrochemical oxygen evolution reaction.

Journal of Materials Chemistry A Accepted Manuscript